TÜBİTAK

Turkish Journal of Earth Sciences

http://journals.tubitak.gov.tr/earth/

Research Article

Turkish J Earth Sci
(2019) 28: 603-622

doi:10.3906/yer-1901-10

Petrography, geochemistry, and provenance of Jurassic sandstones from the Sakarya Zone, NW Turkey

Fırat ŞENGÜN[1,*], **Osman Ersin KORALAY**[2]

[1]Department of Geological Engineering, Faculty of Engineering, Çanakkale Onsekiz Mart University, Çanakkale, Turkey
[2]Department of Geological Engineering, Faculty of Engineering, Dokuz Eylül University, İzmir, Turkey

Received: 09.01.2019 • **Accepted/Published Online:** 29.04.2019 • **Final Version:** 22.07.2019

Abstract: The Jurassic sandstones exposed in the western part of the Sakarya Zone are yellowish to brown, moderate to well sorted, medium to coarse-grained, grain-supported, and cemented by calcareous and minor silica. Sandstones are mainly classified as litharenite, subarkose, and arkose according to the relative proportions of quartz, feldspar and rock fragments, and major element ratios. On the SiO_2 variation diagram, Na_2O and K_2O show slight positive correlations, which could reflect abundance of sodic plagioclase and K-feldspar with quartz within high Si-content sandstones. Sandstones generally exhibit slight LREE enrichment with respect to HREEs. The REE plots are characteristic for sedimentary rocks derived from the upper continental crust. Combining the results of several provenance discrimination diagrams, elemental ratios (Th/Sc, Zr/Sc, La/Th), and REE contents in sandstones, they reveal that the sandstones originated from intermediate to felsic source rocks. Accordingly, the probable source of the Jurassic sandstones is the crystalline basement of the Sakarya Zone consisting of Devonian, Carboniferous, and Permian granitoids, and high-grade metamorphic basement rocks. The Jurassic sandstones mostly have characteristic features of passive continental margin basins. It can be noted that the sandstones may have been deposited in a marginal basin that began to open in Early Jurassic time. CIA and CIW values for the Jurassic sandstones suggest that the source area was subject to low to moderate chemical weathering under semihumid to semiarid climatic conditions.

Key words: Petrography, geochemistry, Jurassic, Sakarya Zone, NW Turkey

1. Introduction

Geochemical analyses of sedimentary rocks are commonly used to determine the relationships between provenance and tectonic setting (e.g., Dickinson, 1970; Dickinson and Suczek, 1979; Bhatia, 1983; Critelli et al., 2003; Tetiker, 2010; Saydam Eker and Korkmaz, 2011; Hara et al., 2012; Saydam Eker, 2012; von Eynatten et al., 2012; Basu et al., 2016). The composition of sedimentary rocks reflects the erosional unroofing, tectonic uplift, and changes in climate and environment. The chemical composition of clastic sedimentary rocks is controlled by the composition of source rocks, hydraulic sorting, chemical weathering during diagenesis, and transport, which are affected by tectonic setting, climate, and the nature of the depositional environment (McCann, 1991; Morton and Hallsworth, 1994; Cox et al., 1995; Ghosh and Sarkar, 2010; Garzanti et al., 2013).

The whole-rock geochemical data in sandstones give more insights about tectonic setting in the sense of discrimination diagrams if the whole-rock chemical composition of a sedimentary rock is not changed (e.g., Nesbitt and Young, 1984; Roser and Korsch, 1986; Periasamy and Venkateshwarlu, 2017). Zr, Hf, Th, Sc, Nb, and Y are the most convenient trace elements for provenance studies owing to the relatively low mobility of these elements and short residence time in sea water during the weathering and sedimentary processes (Cullers, 2000; Young et al., 2013). Therefore, La or Th to Co, Sc, or Cr ratios are sensitive markers for the composition of source rocks (Cullers, 2000).

Several provenance studies have been completed in the Sakarya Zone so far and mostly deal with U-Pb detrital zircon and rutile geochronology, which forms one piece of the sediment provenance puzzle (Ustaömer et al., 2012b; Ustaömer et al., 2016; Akdoğan et al., 2017, 2018). Geochemical and petrographic analyses are a powerful tool to reveal sedimentary processes and provide detailed information about lithological and mineralogical composition of source rocks and tectonic settings. Different tectonic settings with their own rock

* Correspondence: firatsengun@comu.edu.tr

types give rise to clastic rocks with certain compositions when they are eroded. Therefore, the purpose of this paper is to combine sandstone petrography with geochemical analyses to unravel the origin, source rocks, and tectonic setting of Jurassic sandstones from the western part of the Sakarya Zone, which is crucial for the Mesozoic evolution of the Sakarya Zone.

2. Geological setting

The Jurassic sandstones of the Bayırköy Formation form the cover units of the Sakarya Zone. The E-W trending Sakarya Zone is a continental sliver with different oceanic and continental units of different ages. The Sakarya Zone expands from the Biga Peninsula in the west through the Eastern Pontides (Figure 1a), which is bounded by the İstanbul Zone and the Black Sea in the northeast and the Strandja Massif to the north. The Sakarya Zone is separated from the Anatolide-Tauride Block by the İzmir-Ankara-Erzincan suture zone in the south. The Sakarya Zone has a pre-Jurassic basement composed of three distinct tectonic units: (i) medium to high-grade metamorphic basement rocks of the Uludağ Massif, Çamlıca metamorphics, Kazdağ Massif, Kurtoğlu metamorphic complex, and Pulur Massif dated by monazite and zircon minerals, which yield 310–334 Ma (Carboniferous, Okay et al., 2006; Topuz et al., 2007; Ustaömer and Robertson, 2010; Şengün and Koralay, 2017); (ii) granitoids with crystallization ages of Devonian, Carboniferous, and Permian (Okay et al., 1996, 2006; Topuz et al., 2004, 2010; Dokuz, 2011; Aysal et al., 2012a, 2012b; Sunal, 2012; Ustaömer et al., 2012b; Kaygusuz et al., 2016); and (iii) the Permo-Triassic Karakaya Complex, consisting of the lower Karakaya Complex and upper Karakaya Complex (Okay and Göncüoğlu, 2004). The lower Karakaya Complex chiefly consists of greenschist-facies metamorphic rocks with Late Triassic eclogites and blueschist, which forms part of the Paleotethys oceanic crust. The upper Karakaya Complex is chiefly composed of successions of highly deformed clastic and volcanic rocks comprising Carboniferous and Permian limestone exotic blocks and Permian to Late Triassic radiolarian cherts tectonically overlying low-grade metamorphic rocks. Lower Jurassic volcanic and sedimentary successions unconformably overlie the basement rocks of the Sakarya Zone. They are composed of conglomerate, sandstone, shale of fluvial to shallow marine character, and shale (Altıner et al., 1991).

2.1. Stratigraphy of the Bayırköy Formation

Jurassic sandstones of the Bayırköy Formation are exposed in four different regions in the western part of the Sakarya Zone (Figure 1b). These areas are Gönen, Karacabey, Mustafa Kemal Paşa, and Bilecik. The Bayırköy Formation generally consists of conglomerate, sandstone, shale, and claystone, and it is unconformably overlain by the Bilecik limestone (Figures 2a–2d). The age of Bayırköy Formation is Sinemurian-Early Pliensbachian according to fossils from red nodular ammonitico rosso limestones intercalated within the clastic rocks (Altıner et al., 1991).

Jurassic sequences unconformably overlie the Karakaya Complex with greenschist-facies metamorphic rocks in the Gönen area (Figure 2a). The sedimentary succession (~150 m thick) is transgressive and mainly consists of sandstone with alternations of conglomerate, siltstone, and marl. It starts with coarse-grained conglomerate at the bottom and passes up to medium to coarse-grained sandstone. Fine-grained marl occurs on top of the Bayırköy Formation. Clast- to matrix-supported conglomerates are characterized by reddish yellow color, coarse grain size, cross-bedding, and well-sorted pebbles consisting of limestone, quartzite, sandstone, granite, and basalt. Predominant sandstone layers appear light brown, medium to coarse-grained, and well-bedded in the field (Figure 3a). Shale layers of 2–4 cm in thickness occur among sandstone layers 10–20 cm thick (Figure 3b).

The Bayırköy Formation has a thickness of ~100 m in the Karacabey region and unconformably overlies Devonian granite (Figure 2b). The lower part of the formation is characterized by gray-colored, coarse-grained, well-sorted, and clast-supported conglomerates with thicknesses of 1–2 m (Figure 3c). These pebbles mainly comprise sandstone, claystone, limestone, and schist and their sizes range between 0.4 cm and 10 cm. The conglomerates pass gradually upward into yellowish brown-colored, medium to coarse-grained, and thick-bedded sandstones. The best outcrops of these sandstones are observed in the Akçakoyunlu and Kıranlar villages. Fine-grained, greenish gray-colored claystone occurs in the uppermost part of the Jurassic clastic succession.

The clastic units of the Bayırköy Formation chiefly consist of conglomerate, sandstone, shale, and marl in the Mustafa Kemal Paşa region (Figure 2c). The Bayırköy Formation has thickness of ~200 m and unconformably overlies the unmetamorphosed clastic rocks with limestone blocks of the Karakaya Complex in the studied region. A thickness of ~15 m of reddish brown-colored, coarse -grained, clast-supported conglomerates occurs in the lowest part of the formation and gradually changes upward into sandstone and shale intercalations with a thickness of ~150 m. The sandstones are observed as yellowish brown-colored, medium to coarse-grained, thick-bedded, and cross-stratified. The grain size of the sandstone decreases upward and gradually passes into green, yellow-colored, fine-grained, and thin-bedded shale. The uppermost part of the formation is represented by ~40 m of whitish, gray-colored, fine-grained, thin-bedded marl.

The Bayırköy Formation consists predominantly of sandstone and shale intercalations in the Bilecik area with a thickness of up to 250 m (Figure 2d). This unit rests unconformably over granitic basement and starts

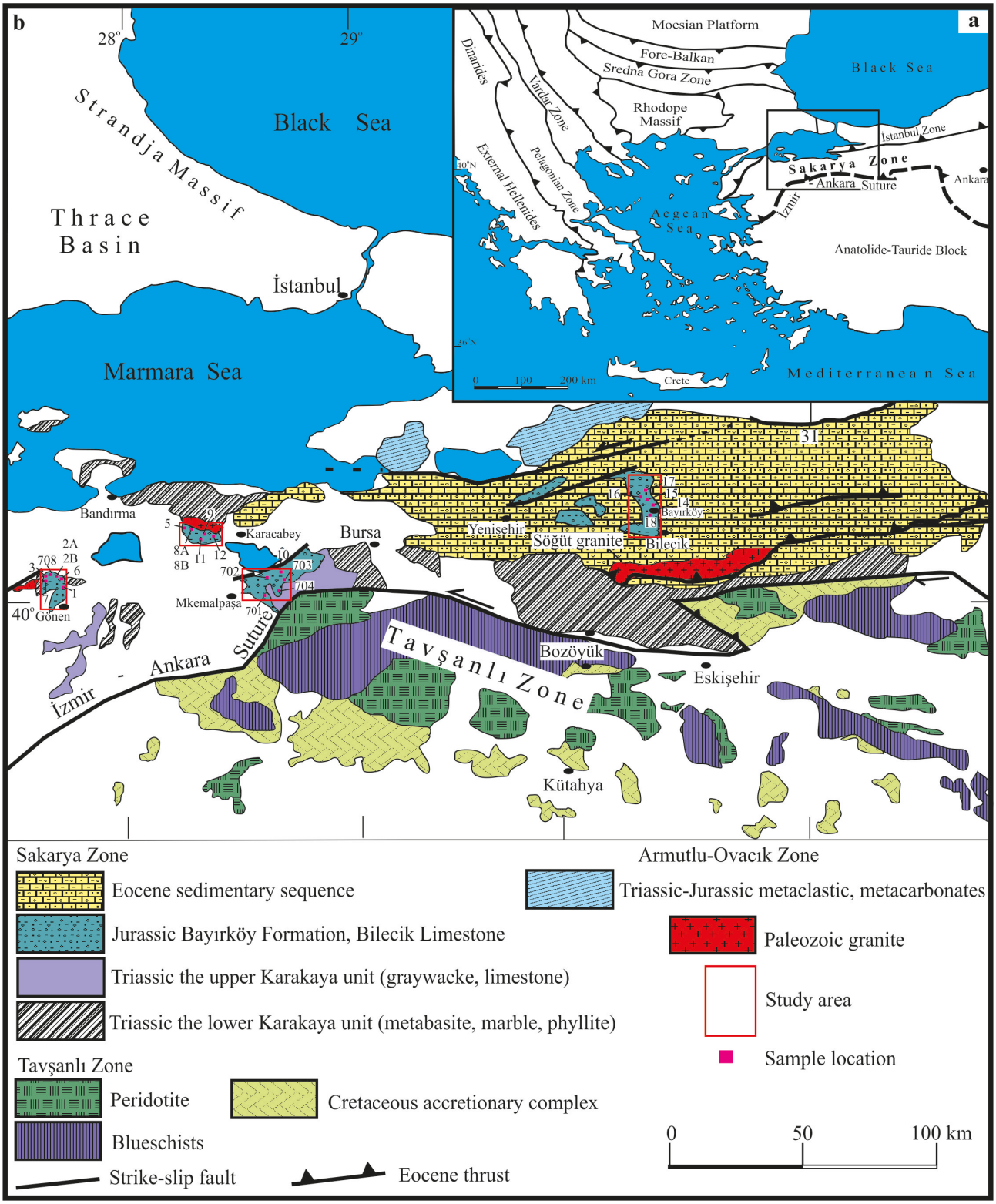

Figure 1. (a) Simplified geotectonic map of the Eastern Mediterranean region (after Okay and Tüysüz, 1999; Meinhold et al., 2010). (b) Geological map of northwest Turkey showing the distribution of Mesozoic rocks with the sample locations (modified from Okay et al., 2006).

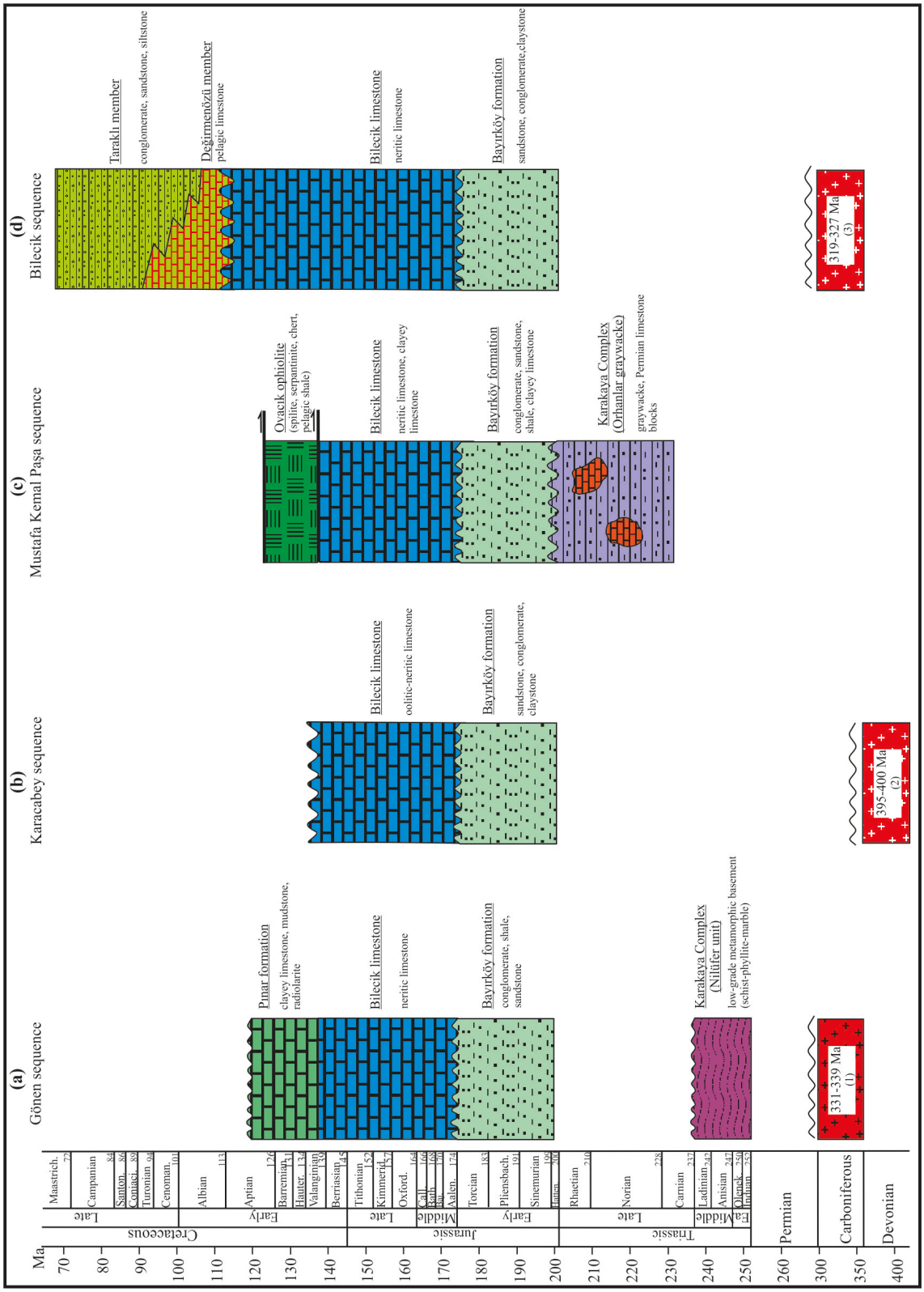

Figure 2. Generalized stratigraphic sections of Mesozoic sedimentary sequences in western Turkey. Mesozoic sequences were modified from Yiğitbaş et al. (2009) (a, b), Kandemir et al. (2013) (c), and Duru et al. (2002) (d). U-Pb zircon geochronology: 1, Şengün (2019); 2, Aysal et al. (2012a), Sunal (2012); 3, Ustaömer et al. (2012a).

Figure 3. Field photographs from the Bayırköy Formation. (a) Close-up view of brown-colored, medium to coarse-grained sandstone (35S 0545872N–4447840E); (b) thick-bedded sandstone and thin-bedded shale alternation (35S 0545484N–4447377E); (c) conglomerate from the lowest part of the Bayırköy Formation (35S 0616117N–4456924E). Pebbles are usually well-sorted limestone and sandstone. (d) View of contact between the Bayırköy Formation and Bilecik Limestone (35S 0245621N–4464865E). The contact relationship between them is unconformable.

with yellowish brown, medium-bedded, fine to medium-grained sandstone. It continues upward with metric alternations of greenish yellow-colored, fine-bedded, and fine-grained shale. The lower part of this unit represents a terrestrial environment and the upper parts reflect a shallow marine environment (Duru et al., 2002).

The Bayırköy Formation is unconformably overlain by the Bilecik limestone in the four studied areas in the western Sakarya Zone. Fossil assemblages of gastropods, ammonites, belemnites, bivalves, crinoids, brachiopods, and foraminifera were identified and assigned Sinemurian-Pliensbachian age for this unit (Altınlı, 1973; Altıner et al., 1991; Akyürek et al., 1996).

3. Sampling and analytical methods

3.1. Sampling

Forty-two sandstone samples were collected from the Gönen (13), Karacabey (11), Mustafa Kemal Paşa (9), and Bilecik (9) areas for petrographic studies and major, trace, and rare earth element analyses. Table 1 shows the sample list and corresponding GPS coordinates.

Nineteen sandstone samples were prepared for thin sections and analyzed by using a polarized microscope with a point-counting stage. Sandstone composition was evaluated by point-counting 350 grains for each sandstone using the Gazzi–Dickinson counting method (Ingersoll

Table 1. Sample locations and corresponding coordinates (WGS84).

Sample no.	Lithology	Location	N	E
1	Subarkose	Gönen (Balıkesir)	35S 0546666	35S 4445380
2A	Arkose	Gönen (Balıkesir)	35S 0545943	35S 4447847
2B	Subarkose	Gönen (Balıkesir)	35S 0545943	35S 4447847
3	Litharenite	Gönen (Balıkesir)	35S 0446968	35S 4747370
6	Litharenite	Gönen (Balıkesir)	35S 0547496	35S 4447712
7	Litharenite	Gönen (Balıkesir)	35S 0544735	35S 4447551
708	Litharenite	Gönen (Balıkesir)	35S 0544816	35S 4447836
5	Subarkose	Karacabey (Bursa)	35S 0612111	35S 4458686
8A	Litharenite	Karacabey (Bursa)	35S 0614035	35S 4458344
8B	Litharenite	Karacabey (Bursa)	35S 0614035	35S 4458344
9	Subarkose	Karacabey (Bursa)	35S 0616210	35S 4456975
11	Subarkose	Karacabey (Bursa)	35S 0616222	35S 4457048
12	Litharenite	Karacabey (Bursa)	35S 0616588	35S 4457656
10	Subarkose	Mustafa Kemal Paşa (Bursa)	35S 0634635	35S 4438956
701	Litharenite	Mustafa Kemal Paşa (Bursa)	35S 0637268	35S 4436511
702	Litharenite	Mustafa Kemal Paşa (Bursa)	35S 0634982	35S 4436041
703	Litharenite	Mustafa Kemal Paşa (Bursa)	35S 0634923	35S 4437936
704	Litharenite	Mustafa Kemal Paşa (Bursa)	35S 0635100	35S 4437845
14	Litharenite	Bilecik	35S 0246374	35S 4464310
15	Litharenite	Bilecik	35S 0245732	35S 4464768
16	Arkose	Bilecik	35S 0245621	35S 4464865
17	Litharenite	Bilecik	35S 0244978	35S 4463389
18	Litharenite	Bilecik	35S 0246720	35S 4463610

et al., 1984; Stunner and Basu, 1985). Cement and matrix were estimated with visual percentage estimation.

3.2. Analytical methods

Twenty-three representative sandstone samples (7 samples from the Gönen area, 6 samples from the Karacabey area, 5 samples from the Mustafa Kemal Paşa area, and 5 samples from the Bilecik area) were analyzed for whole-rock geochemical data. The sample locations are presented in Figure 1b. Geochemical analyses of major, trace, and rare earth elements were obtained from ALS Chemex Laboratory in Canada. Major element concentrations were determined by inductively coupled plasma-atomic emission spectroscopy (ICP-AES). Trace element and REE concentrations were analyzed by inductively coupled plasma-mass spectroscopy (ICP-MS). The prepared sample (0.200 g) was added to lithium metaborate/lithium tetra borate flux (0.90 g), mixed well, and fused in a furnace at 1000 °C. The resulting melt was then cooled and dissolved in 100 mL of 4% nitric acid and 2% hydrochloric acid. This solution was then analyzed by ICP-AES and the results were corrected for spectral interelement interference. The oxide concentration was calculated from the determined elemental concentrations.

4. Results

4.1. Sandstone petrography

The Jurassic sandstones from the Bayırköy Formation are predominantly yellowish to brown-colored, moderate to well-sorted, medium to coarse-grained, and grain-supported. Sandstone clasts are chiefly composed of quartz, K-feldspars, and rock fragments. Zircon, rutile, and apatite minerals occur as accessory mineral phases. Mineralogical composition of the sandstones is given in Table 2. Sandstones are classified as mostly litharenite, subarkose, and arkose according to quartz, feldspar, and rock fragment proportions (Figure 4a). The geochemical classification diagram provides the same results based on major element ratios for SiO_2/Al_2O_3 vs. Na_2O/K_2O (Pettijohn et al., 1972) (Figure 4b).

Quartz is a dominant framework grain in most sandstone samples and occurs as both monocrystalline

Table 2. Mineralogical composition and point-counting results of Jurassic sandstones from the Bayırköy formation. Values are given in %.

Location	Gönen						Karacabey					Mustafa Kemal Paşa				Bilecik			
Grain size	Medium to coarse	Medium to coarse	Medium to coarse	Medium to coarse	Fine to medium	Fine to medium	Medium to coarse	Medium to coarse	Medium to coarse	Medium to coarse	Medium to coarse	Medium to coarse	Fine to medium	Medium to coarse	Medium to coarse	Medium to coarse	Medium to coarse	Medium to coarse	Medium to coarse
Sample no.	1	2A	2B	6	7	708	1705B	8A	8B	9	1711B	10	701	702	703	14	15	17	18
Quartz																			
Monocrystalline	38.5	42.7	45.2	45.3	36.7	41.5	59.2	42.5	64.1	40.6	33.5	36.2	35.6	42.2	37.7	63	48.1	33.5	48.7
Polycrystalline	4.8	5.6	7.2	8.2	3.6	5.3	7.4	8	6.1	10.7	7.8	9.2	6.6	9.8	8.2	6.6	7.3	8.4	5.3
Total quartz	43.3	48.3	52.4	53.7	40.3	46.8	66.6	50.5	70.2	51.3	43.3	45.4	42.2	52	45.9	69.6	55.4	41.9	54
Feldspar																			
Plagioclase	3.9	2.8	2.4	3.2	4.1	8.9	6.5	2.6	4.8	3.2	5.4	6.5	2.6	3.6	4.2	2.8	3.7	3.4	2.7
Alkali feldspar	7	5.9	2.7	3.7	4.4	10.6	9.6	4.7	7.5	4.2	5.6	6.8	4.4	6,0	7.6	4.9	4.4	6.9	4.6
Total feldspar	10.9	8.7	5.1	6.9	8.5	19.5	16.1	7.3	12.3	7.4	11	13.3	7	9.6	11.8	7.7	8.1	10.3	7.3
Rock fragments	30.5	28.2	27.4	28.8	3.4	3.4	5.5	28.1	4.1	27.4	30.3	29.2	29.6	30.7	32.9	4.2	17.5	27.3	25.5
Other minerals																			
Muscovite	1.2	trace	1.2	0.8	trace	trace	0.7	1.7	trace	1.8	2.7	0.5	1.8	0.6	trace	1.1	trace	trace	trace
Biotite	0.6	trace	trace	trace	0	trace	1	trace	1.6	2.7	3.3	0.9	1.8	trace	1.5	trace	trace	2.2	1.1
Chlorite	1.4	0.9	1.3	trace	trace	trace	trace	0.8	0.6	1.5	1.7	0.7	0.8	trace	0.9	0.8	trace	0.9	trace
Opaques	1.3	0.6	trace	trace	trace	trace	0.5	0.7	trace	trace	0.5	trace	0.6	trace	0.6	trace	trace	trace	trace
Heavy minerals	0.7	0.7	1	trace	trace	trace	trace	trace	trace	trace	trace	trace	trace	trace	trace	trace	trace	trace	1.0
Total of other minerals	5.2	2.2	3.5	0.8	0	0	2.2	3.2	2.2	6	8.2	2.1	5	0.5	3	1.9	0	3.1	2.1
Cement																			
Silica	0	4.1	1.2	0	0	2.7	9.3	1.2	3.4	0	7.2	5.4	8.2	7.1	6.4	4.2	5.6	0	3.7
Carbonate	10.1	8.5	10.4	9.8	38.8	27.6	0	8.5	9.1	7.9	0.0	4.1	0	0	0	10.4	13.4	17.4	7.4
Total cement	10.1	12.6	11.6	9.8	37.8	30.3	9.3	9.7	12.5	7.9	7.2	9.5	8.2	7.1	6.4	14.6	19	17.4	11.1
Total of all constituents	100	100	100	100	100	100	100	100	100	100	100	100	100	100	100	100	100	100	100

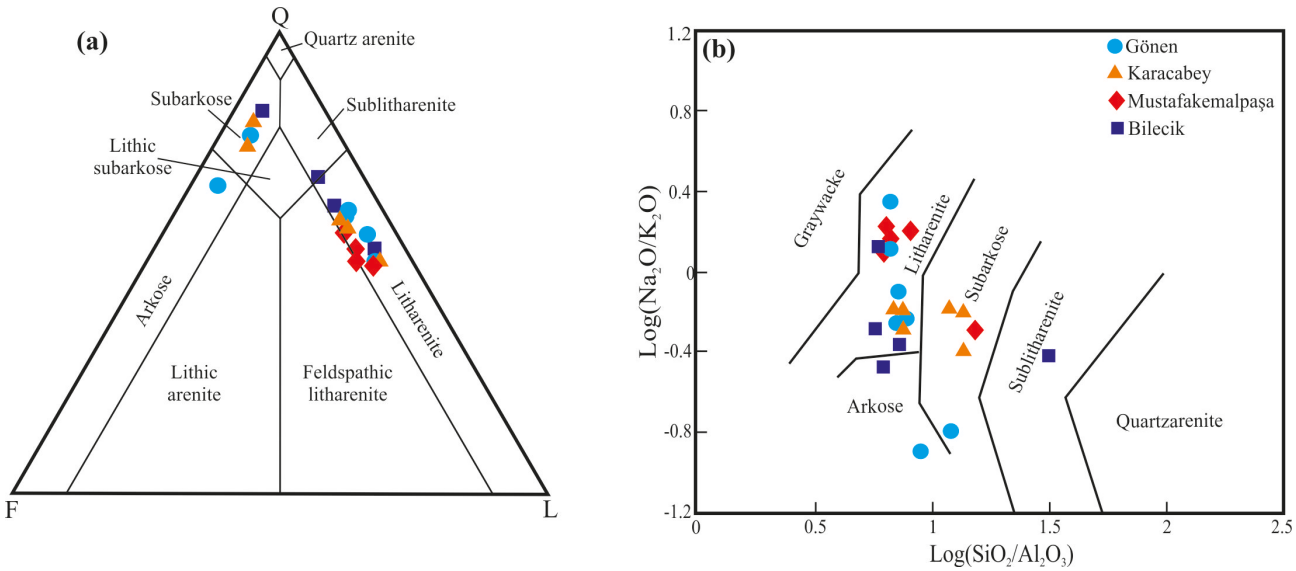

Figure 4. (a) Triangular QFL diagram for sandstone classification (after McBride, 1963). Q: Quartz, F: feldspar, L: lithic fragments. (b) Chemical classification diagram for the sandstone samples (after Pettijohn et al., 1972).

grains (Qm) and polycrystalline grains (Qp). Subangular monocrystalline quartz is the most abundant component (44%) of sandstone samples and exhibits straight to slightly undulose extinction (Figure 5a). Polycrystalline quartz (7%) includes 2–3 subgrains with uniform extinction showing volcanic source (Tucker, 1991, Figure 5b). Polycrystalline grains with 2–3 subgrains have straight to slightly curved intercrystalline boundaries. However, the polycrystalline grains with more than 5 crystals have elongated shape and display undulose extinction with irregular to crenulated intercrystalline boundaries. Polycrystalline quartz with more than 3 subgrains and undulose extinction shows derivation from metamorphic source rocks (Lewis and McConchie, 1994). K-feldspar and plagioclase grains generally have subrounded to subangular shape and constitute 12% of the sandstones, and they are widely replaced by sericite (Figure 5c). Petrographic studies indicate that plagioclase grains occur less abundantly than K-feldspar, which is attributed to either durability of K-feldspar or the lack of plagioclase-bearing source rocks (Zaid et al., 2015). K-feldspar has Carlsbad twinning, whereas plagioclase is characterized by polysynthetic twinning. Rock fragments (22%) are mainly composed of a mix of volcanic (Lv), metamorphic (Lm), and sedimentary rock fragments (Lc). Volcanic rock fragments are composed of fine-grained basaltic/andesitic rock fragments with oriented fine plagioclase laths (Figure 5d). Metamorphic rock fragments are generally composed of polycrystalline quartz grains originating from high-grade metamorphic sources (Figure 5e). Metamorphic polycrystalline quartz with recrystallized subgrains is oriented and exhibits undulose extinction. Sedimentary rock fragments, especially chert, are very common in the sandstone samples (Figure 5f). The Jurassic sandstones are cemented by silica and carbonate with amounts varying from 4% to 10%.

4.2. Major and trace elements

Sandstones from the four areas have changeable geochemical compositions, especially in major element concentrations (Gönen, Karacabey, Mustafa Kemal Paşa, and Bilecik). Table 3 shows major oxides and trace element contents of the sandstones. Samples are characterized by moderate to high K_2O (0.49%–3.99%), low to high SiO_2 (56%–86%), low to moderate Al_2O_3 (2%–12%) and Na_2O (0.3%–2.99%), and low Fe_2O_3 (0.96%–5%). A sample (15) from the Bilecik area has the highest SiO_2 content (86%) and the lowest Fe_2O_3 content (0.96%). Samples (2A, 2B from Gönen area and 18 from Bilecik area) are enriched in K_2O (3.29%–3.99%), which suggests that K-rich feldspar is abundant in their mineralogical composition. The combination of high Al_2O_3 and Na_2O concentrations documents abundant albite components for sample no. 03 (Gönen) and sample no. 704 (Mustafa Kemal Paşa), as confirmed by petrographic observations. In other words, high Al_2O_3 values could result from K-feldspar and mica content in sandstones. High values of CaO (10.1%–17%) and LOI (6.7%–13%) for sandstone samples (1, 6, 7, and 708 from Gönen; 13 from Karacabey; and 17 from Bilecik) show the presence of carbonate-bearing phases.

Harker variation diagrams exhibit clear correlations for major and trace elements (Figure 6). Al_2O_3 and Fe_2O_3 contents indicate negative correlations on the SiO_2 variation

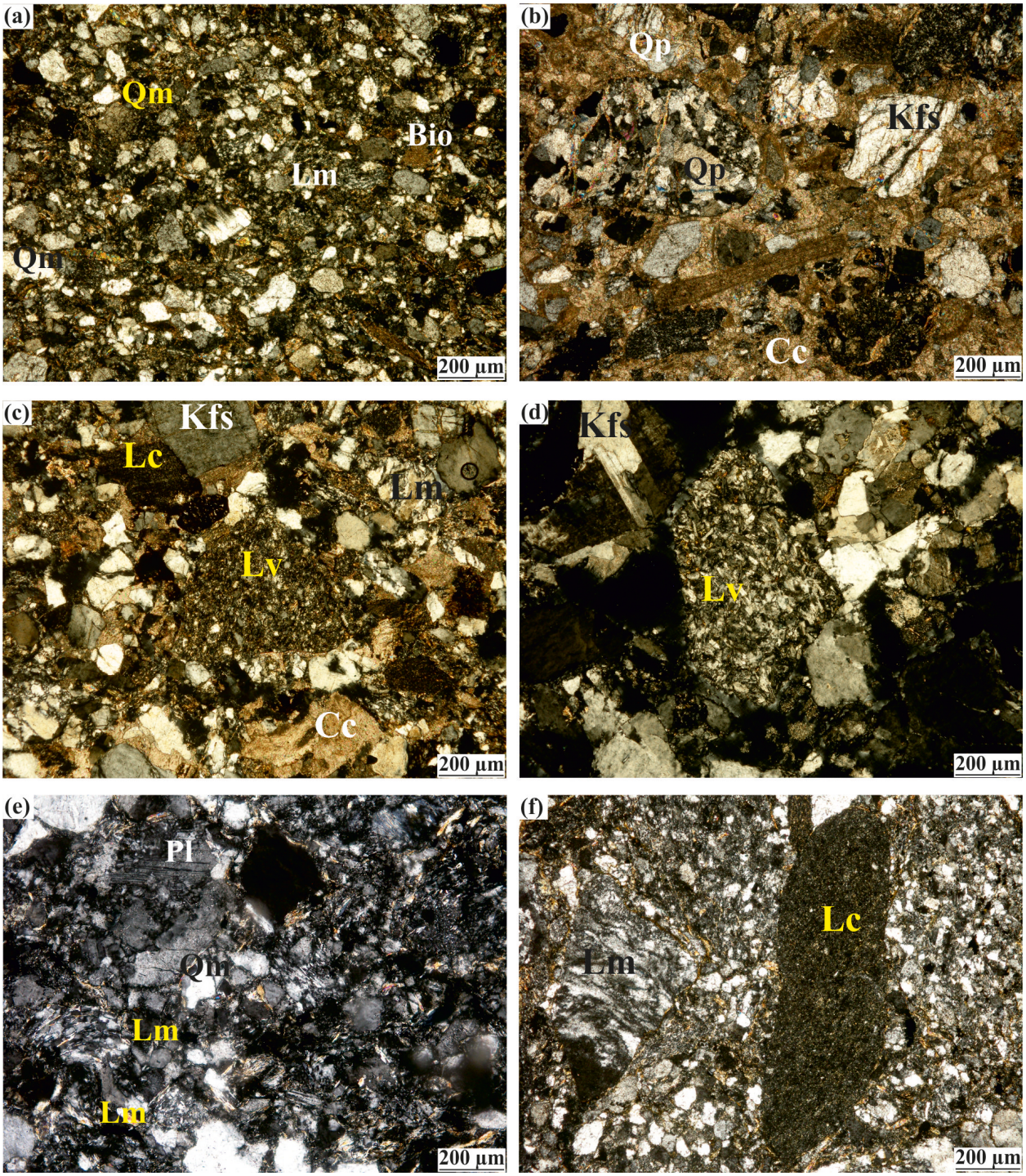

Figure 5. Photomicrographs of selected Jurassic sandstones in cross-polarized light. (a) Subarkosic sandstone with subrounded monocrystalline quartz grains with straight extinction (sample no. 14 from Bilecik). (b) Polycrystalline quartz grain showing a number of subgrains with straight to slightly curved intercrystalline boundaries (sample no. 702 from Mustafa Kemal Paşa). (c) Arkosic sandstone with subrounded to subangular feldspar grains cemented by carbonate matrix (sample no. 8B from Karacabey). (d) Volcanic rock fragments with basaltic/andesitic origin (sample no. 2A from Gönen). (e) Metamorphic fragments represented by quartz grains (sample no. 10 from Mustafa Kemal Paşa). (f) Subangular chert grains forming the most common rock fragments (sample no. 703 from Mustafa Kemal Paşa). Qm: Monocrystalline quartz, Qp: polycrystalline quartz, Kfs: potassium feldspar, Pl: plagioclase, Bt: biotite, Cal: calcite, Lv: volcanic fragment, Lm: metamorphic fragment, Lc: sedimentary fragment; mineral abbreviations after Kretz (1983).

Table 3. Chemical composition of major elements (wt.%) and trace elements (ppm) of sandstones from the Bayırköy Formation.

Location	Gönen							Karacabey						Mustafa Kemal Paşa						Bilecik			
Sample no.	1	2A	2B	3	6	7	708	5	8A	8B	9	11	13	10	701	702	703	704	14	15	16	17	18
Major elements (wt.%)																							
SiO_2	62.60	81.00	79.20	79.70	61.50	64.60	65.20	75.10	65.80	74.40	79.00	75.60	69.10	74.70	73.90	62.10	78.70	74.70	73.60	86.00	74.60	56.10	71.00
Al_2O_3	8.09	11.20	11.25	12.05	9.18	5.32	7.28	5.50	8.76	6.26	10.60	10.90	5.08	11.30	11.50	4.09	9.62	12.20	11.85	2.71	10.10	9.27	12.20
tFe_2O_3	1.94	1.44	1.92	1.62	2.86	2.25	2.49	2.12	2.59	2.24	2.80	3.03	1.29	4.46	5.00	1.18	4.62	4.79	4.15	0.96	3.98	4.22	4.18
CaO	11.30	0.29	0.45	0.43	16.80	15.60	10.10	8.90	9.37	7.24	0.44	1.51	12.00	0.41	0.30	17.00	0.21	0.34	1.30	3.20	4.10	14.25	1.97
MgO	0.16	0.16	0.34	0.18	0.24	0.81	0.88	0.43	0.71	0.58	0.87	1.01	0.32	1.38	1.54	0.33	1.23	1.44	0.45	0.35	1.27	1.23	1.04
Na_2O	1.12	2.91	2.22	2.99	1.11	0.26	0.30	0.86	1.14	0.98	1.86	1.89	0.77	2.24	2.48	0.71	2.02	2.28	1.00	0.43	0.72	2.08	1.73
K_2O	1.87	3.56	3.99	2.27	0.49	1.58	2.32	1.31	2.12	1.41	2.79	2.79	1.83	1.50	1.44	1.35	1.23	1.77	2.97	1.12	1.64	1.59	3.29
Cr_2O_3	0.01	0.01	0.01	0.01	0.01	0.01	0.01	0.01	0.01	0.01	0.01	0.01	0.01	0.01	0.01	0.01	0.01	0.01	0.01	0.01	0.02	0.01	0.01
TiO_2	0.26	0.28	0.20	0.12	0.25	0.26	0.36	0.18	0.36	0.32	0.38	0.47	0.12	0.64	0.65	0.07	0.59	0.71	0.45	0.05	0.48	0.34	0.38
MnO	0.10	0.02	0.03	0.03	0.24	0.15	0.13	0.33	0.18	0.13	0.05	0.07	0.13	0.05	0.07	0.05	0.06	0.07	0.05	0.04	0.31	0.13	0.04
P_2O_5	0.03	0.01	0.05	0.07	0.04	0.09	0.09	0.07	0.06	0.05	0.08	0.10	0.06	0.14	0.12	0.04	0.14	0.15	0.07	0.03	0.12	0.07	0.03
SrO	0.05	0.01	0.02	0.03	0.01	0.01	0.01	0.01	0.03	0.01	0.01	0.01	0.01	0.02	<.01	0.01	0.01	0.01	0.01	0.03	0.01	0.02	0.01
BaO	0.10	0.02	0.08	0.03	0.02	0.02	0.02	0.04	0.05	0.04	0.05	0.05	0.19	0.03	0.03	0.04	0.03	0.04	0.07	0.02	0.04	0.04	0.08
LOI	10.85	1.11	1.79	1.76	6.70	9.80	12.00	6.30	9.75	7.95	2.52	3.54	8.10	2.51	2.44	13.00	2.17	2.95	4.56	6.00	3.10	10.30	5.62
Total	98.47	101.80	101.54	101.28	99.44	100.76	101.18	101.15	100.93	101.62	101.46	100.97	98.99	99.39	99.48	99.97	100.63	101.45	100.53	100.94	100.48	99.65	101.57
CaO*	1.12	0.29	0.45	0.43	1.11	0.26	0.30	0.86	1.14	0.98	0.44	1.51	0.77	0.41	0.30	0.71	0.21	0.34	1.00	0.43	0.72	2.08	1.73
SiO_2/Al_2O_3	7.74	7.23	7.04	6.61	6.70	12.14	8.96	13.65	7.51	11.88	7.45	6.94	13.60	6.61	6.43	15.18	8.18	6.12	6.21	31.73	7.39	6.05	5.82
tFe_2O_3/Al_2O_3	0.24	0.13	0.17	0.13	0.31	0.42	0.34	0.39	0.30	0.36	0.26	0.28	0.25	0.39	0.43	0.29	0.48	0.39	0.35	0.35	0.39	0.46	0.34
CIA	66.31	62.36	62.81	67.93	77.21	71.70	71.37	64.48	66.57	65.01	67.56	63.78	60.12	73.14	73.16	59.62	73.55	73.54	70.45	57.78	76.63	61.72	64.38
CIW	87.84	79.38	83.52	80.12	89.21	95.34	96.04	88.48	86.46	85.07	86.48	85.22	86.84	83.46	82.26	85.21	82.65	84.25	92.22	86.31	93.35	81.67	87.58

Total iron expressed as tFe_2O_3. Chemical index of alteration (CIA) = $(Al_2O_3/(Al_2O_3+CaO^*+Na_2O+K_2O) \times 100$ (Nesbitt and Young, 1982); CIW = $(Al_2O_3/Al_2O_3+CaO^*+Na_2O) \times 100$ (Harnois, 1988). CaO* = CaO in silicate fraction.

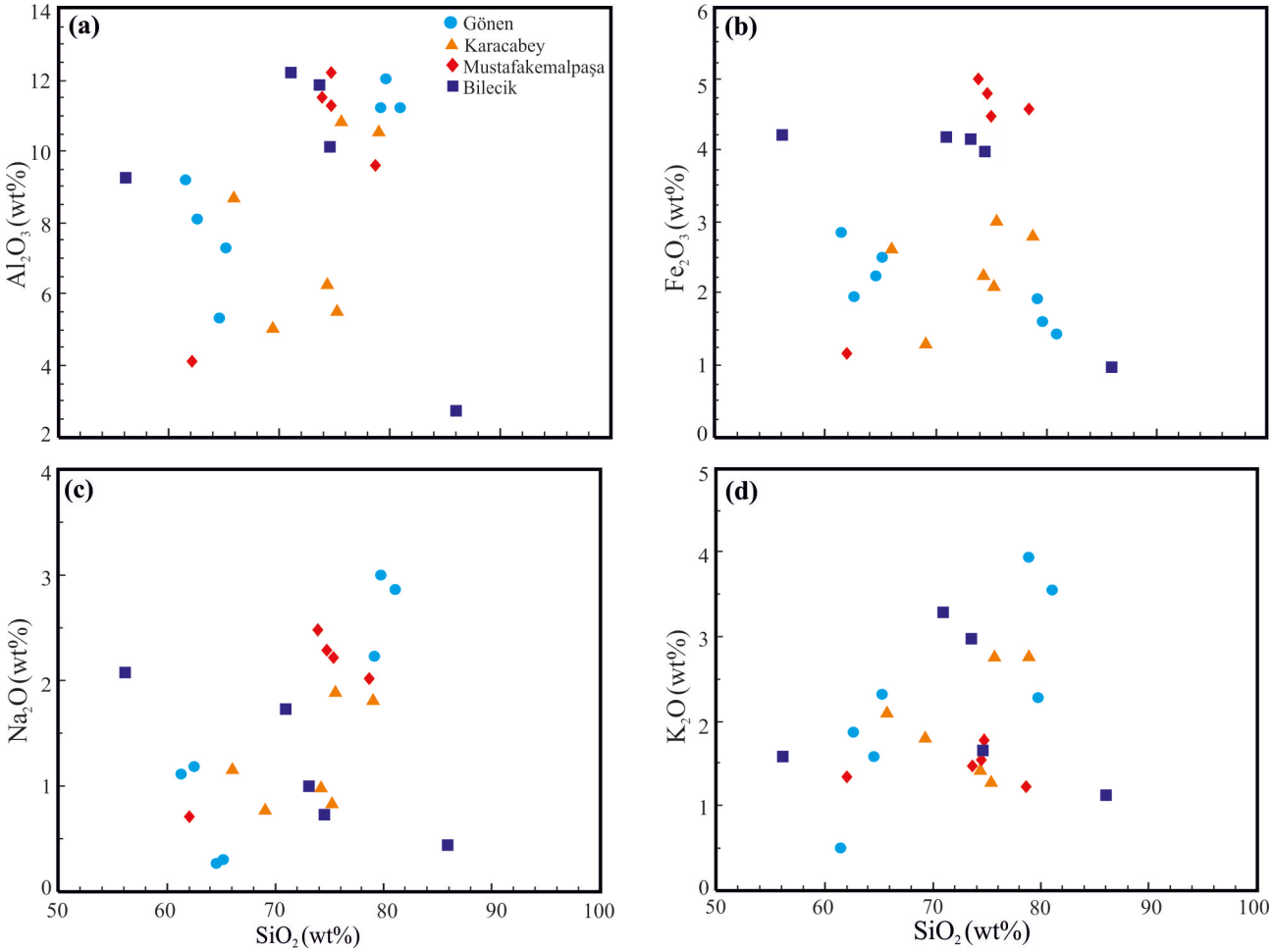

Figure 6. Correlation diagrams of Al_2O_3, Fe_2O_3, K_2O, and Na_2O versus SiO_2.

diagram (Figures 6a and 6b). These negative correlations probably reflect changing illite-rich clay minerals, quartz, and muscovite ratios in the primary source rocks. Na_2O and K_2O show slightly positive correlations (Figures 6c and 6d), which can reflect the abundance of sodic plagioclase and K-feldspar with quartz in high Si-content sandstones.

Trace element concentrations of the sandstones are heterogeneous and distributed in wide ranges (Table 3). The concentrations of trace elements from sandstones are presented on a multielement diagram (Figure 7a) and are indistinctly below the upper continental crust (UCC) level. The large-ion lithophile elements (LILEs) (Rb, Ba, Sr, Th, U) are compared to the UCC, in which Sr (61.4–375 ppm) and Rb (22.3–108.5 ppm) are depleted with minor enrichment of Th (2.12–12.65 ppm) in sandstone samples (Figure 7a). Incompatible and easily mobilized LILE concentrations are usually controlled by the existence/lack of feldspar, and LILEs show enrichment in the UCC compared with the mantle (Löwen et al., 2018). The incompatible high field-strength elements (HFSEs) are considered to be relatively immobile elements and thus could give additional information for the provenance of the sedimentary rocks (Taylor and McLennan, 1985). Zr, Hf, and Y (HFSEs) concentrations are relatively similar to those of the UCC. Sandstone samples show depletion in Nb and lower Nb content (2.6–10.9 ppm) than in the UCC.

4.3. Rare earth elements (REEs)

Chondrite-normalized REE patterns illustrate that the Jurassic sandstones generally exhibit slight light rare earth element (LREE) enrichment with respect to heavy rare earth elements (HREEs) (Figure 7b). Rare earth element (REE) contents for sandstones are given in Table 4. Most of the sandstone samples display slightly flat HREE plots. The REE pattern is characteristic of sedimentary rocks derived from the UCC (McLennan, 1993). Chondrite-normalized La_N/Yb_N ranges between 6.08 and 11.32 (average: 8.84). These sandstone samples have Eu/Eu* values of less than

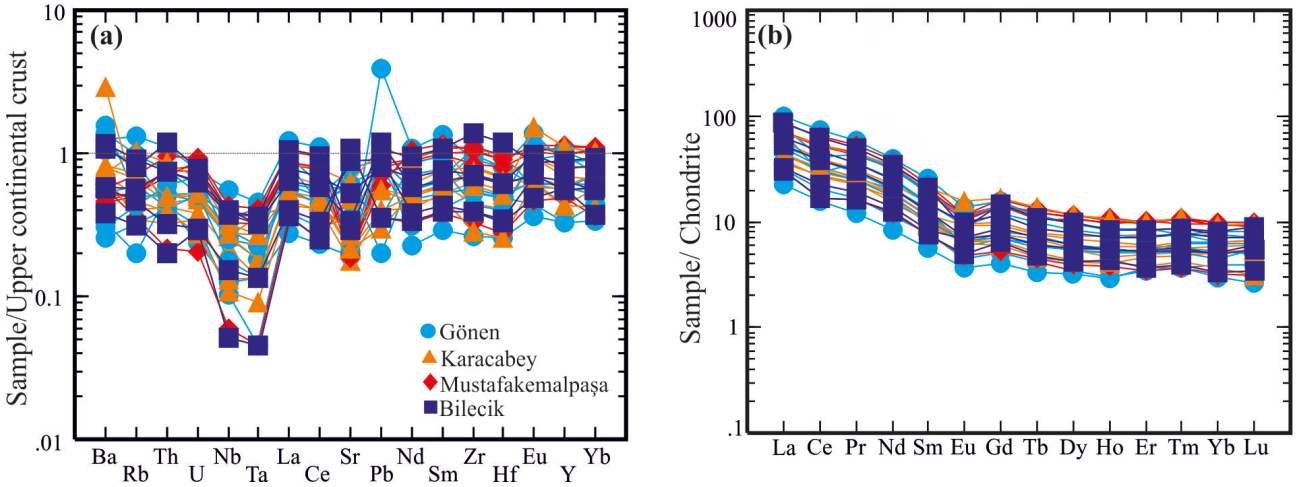

Figure 7. (a) Upper continental crust (UCC)-normalized trace element diagram for sandstone samples. (b) Chondrite-normalized rare earth element (REE) diagram for sandstone samples (normalizing values from Taylor and McLennan, 1985).

0.85, which is typical for sedimentary rocks derived from the UCC. Negative Eu anomalies (0.5–0.8, average: 0.72) and Gd_N/Yb_N ratios (1.13–2.02) show that these sandstones were formed in post-Archean time (Taylor and McLennan, 1985). Moreover, these negative Europium anomalies could be attributed to the presence or partial weathering of plagioclase. Therefore, crystal fractionation or partial melting of rock causes the removal of feldspar and results in a negative Eu anomaly in melt, which affected the source rocks. Plagioclase fractionation is confirmed by the slight development of negative Eu anomalies (Figure 7b).

5. Discussion

5.1. Source rock and provenance of the Jurassic sandstones

Petrographic and geochemical studies were completed to reveal source rocks and provenance of sandstones from the Bayırköy Formation. Petrographic studies show that sandstone samples comprise two distinct types of quartz grains. The first type consists of monocrystalline quartz grains, which are dominant and have straight undulose extinction. This indicates derivation from a plutonic source (Figure 5a). The second type is composed of polycrystalline quartz grains, which are divided into 2 subgrains. The first subgrain includes 2–3 crystals and has straight to slightly curved intercrystalline boundaries. However, polycrystalline grains comprise more than 3 elongate crystals in one grain with irregular intercrystalline boundaries (Figure 5b). The first one is derived from plutonic source rocks but the second type suggests a metamorphic source origin (Asiedu et al., 2000; Zaid et al., 2015). Higher abundance of K-feldspar than plagioclase, muscovite, and biotite indicates a plutonic source.

The composition of the source rock was identified by a discrimination diagram (Roser and Korsch 1988, Figure 8a). This discrimination diagram distinguishes 4 different lithological source areas consisting of mafic, intermediate, felsic igneous, and quartzose sedimentary provenance, which is applied for samples with high CaO content owing to rich carbonate cement in sandstones (Roser and Korsch, 1988). Thus, discrimination functions according to the contents of variable mobile and immobile major elements were normalized to Al_2O_3. The sandstones fall in the intermediate igneous and felsic igneous fields (Figure 8a). This suggests that sediments from the Bilecik and Mustafa Kemal Paşa areas originated from intermediate source rocks and the rest were derived from felsic source rocks.

Ratios of trace elements were used for the potential sources of sandstones (Figures 8b and 8c). The Zr/Sc ratio is a fruitful marker for zircon enrichment and fractionation during sedimentary recycling processes (McLennan and Taylor, 1991). However, the Th/Sc ratio refers to the chemical differentiation in igneous rock processes so that Sc is a compatible element, whereas Th is an incompatible element in igneous rocks and records the provenance of REEs (McLennan, 1989; Borges et al., 2008). Th/Sc and Zr/Sc ratios show trends consistent with igneous differentiation and all samples are near felsic volcanic rocks and average UCC on the Th/Sc vs. Zr/Sc diagram (Figure 8b). This may suggest that the provenance of sandstones is chiefly from felsic volcanic rocks. This is supported by the La/Th against Hf plot (Figure 8c), showing the types of source area. Sandstone samples fall in the acidic arc source field with some intermediate arc sources. The TiO_2 against Ni diagram (Floyd et al., 1991) shows that sandstones originated from acidic source rocks

Table 4. Rare earth element data (ppm) for sandstones from the Bayırköy Formation.

Location	Gönen							Karacabey						Mustafa Kemal Paşa					Bilecik				
Sample no.	1	2A	2B	3	6	7	708	5	8A	8B	9	11	13	10	701	702	703	704	14	15	16	17	18
Rare earth elements (ppm)																							
La	18.00	8.80	18.50	11.30	16.60	25.40	28.40	21.10	15.50	13.00	16.30	16.20	13.80	25.60	25.20	11.00	25.80	30.60	31.80	11.00	23.30	12.00	19.40
Ce	32.00	15.00	36.50	19.70	28.60	28.40	38.90	38.00	29.60	26.30	28.20	31.40	25.60	50.70	48.80	16.00	50.70	61.20	60.70	15.90	43.70	21.80	36.90
Pr	3.56	1.64	3.97	2.32	3.38	4.91	5.89	4.33	3.38	3.16	3.37	3.67	3.10	5.80	5.97	2.18	6.21	7.19	6.76	2.21	4.89	2.58	4.12
Nd	14.30	5.90	14.40	8.10	12.30	18.40	22.60	15.90	12.90	10.70	13.20	13.70	11.90	22.80	22.00	8.50	23.40	27.50	24.50	8.80	17.60	9.80	15.10
Sm	2.88	1.31	3.07	1.83	2.36	3.51	4.24	3.47	2.59	2.39	2.72	2.58	2.19	4.51	4.36	1.72	4.89	5.24	4.79	1.74	3.39	1.95	2.89
Eu	0.53	0.32	0.51	0.39	0.57	0.80	0.99	0.82	0.54	0.54	0.81	0.61	0.55	1.00	0.90	0.41	0.91	1.00	0.76	0.43	0.85	0.60	0.62
Gd	2.48	1.25	2.13	1.54	2.18	3.69	4.45	2.98	2.23	1.83	2.80	2.28	2.00	4.29	4.37	1.60	4.48	4.87	4.42	1.98	3.50	2.33	2.61
Tb	0.42	0.19	0.36	0.24	0.34	0.57	0.68	0.45	0.36	0.27	0.44	0.40	0.30	0.62	0.71	0.26	0.70	0.76	0.64	0.28	0.50	0.35	0.41
Dy	2.27	1.21	1.98	1.29	2.09	3.22	3.59	2.77	2.05	1.60	2.60	2.15	1.64	3.99	4.11	1.51	4.28	4.40	3.71	1.61	2.97	2.14	2.27
Ho	0.48	0.25	0.43	0.26	0.43	0.65	0.73	0.63	0.39	0.34	0.54	0.49	0.35	0.83	0.82	0.32	0.93	0.87	0.70	0.37	0.61	0.46	0.47
Er	1.25	0.92	1.35	0.85	1.25	1.78	2.09	1.86	1.23	1.15	1.52	1.43	0.95	2.52	2.52	0.85	2.49	2.40	2.08	0.91	1.74	1.29	1.33
Tm	0.20	0.13	0.22	0.13	0.18	0.27	0.31	0.26	0.18	0.17	0.20	0.23	0.15	0.34	0.38	0.13	0.38	0.39	0.31	0.14	0.28	0.20	0.19
Yb	1.31	0.88	1.56	0.74	1.12	1.61	1.87	1.86	1.25	1.25	1.46	1.58	0.92	2.38	2.30	0.79	2.41	2.41	2.03	0.81	1.75	1.23	1.27
Lu	0.19	0.15	0.24	0.10	0.21	0.25	0.27	0.27	0.21	0.20	0.23	0.25	0.12	0.34	0.35	0.12	0.37	0.37	0.34	0.13	0.27	0.21	0.23
Y	13.80	7.30	12.60	7.30	12.70	21.30	22.50	16.80	12.20	9.60	15.20	12.90	9.40	21.50	21.70	10.80	24.20	25.10	19.40	12.40	17.40	14.00	12.20
Eu/Eu*	0.61	0.76	0.61	0.71	0.77	0.68	0.70	0.78	0.69	0.79	0.90	0.77	0.80	0.70	0.63	0.76	0.59	0.61	0.50	0.71	0.75	0.86	0.69
(La/Yb)N	9.86	6.08	8.51	10.95	10.63	11.32	10.89	8.14	8.89	7.46	8.01	7.35	10.76	7.72	7.86	9.99	7.68	9.11	11.24	9.74	9.55	7.00	10.96
(Gd/Yb)N	1.57	1.17	1.13	1.72	1.61	1.90	1.97	1.32	1.48	1.21	1.59	1.19	1.80	1.49	1.57	1.67	1.54	1.67	1.80	2.02	1.65	1.57	1.70
(La/Sm)N	4.04	4.34	3.89	3.99	4.54	4.67	4.33	3.93	3.87	3.51	3.87	4.06	4.07	3.67	3.73	4.13	3.41	3.77	4.29	4.08	4.44	3.98	4.34

(Figure 8d). Two sandstone samples from the Karacabey and Bilecik areas are inside the mature sediments area, which is interpreted as the influence of cycling.

Elemental ratios like Eu/Eu*, Th/Sc, La/Sc, La/Co, and Th/Co for sandstones are crucially distinct in mafic and felsic rocks (Cullers, 2000). Thus, they give important insights into the provenance of sedimentary rocks (Taylor and McLennan, 1985). These elemental ratios can be compared to sedimentary rocks derived from felsic and mafic sources, which suggests that all elemental ratios in the Jurassic sandstones occur in the range of sedimentary rocks originating from felsic sources (Table 5). Most samples (9 from the Karacabey area, 17 from the Bilecik area), except for 2 sandstones, plot in the post-Archean field on the Eu/Eu* vs. $(Gd/Yb)_N$ diagram (Figure 9). Moreover, the average value of Eu/Eu* (0.71) falls within the characteristic range of post-Archean sedimentary rocks (Taylor and McLennan, 1985). It could be meaningful for felsic rocks of the post-Archean, which can act like source rock.

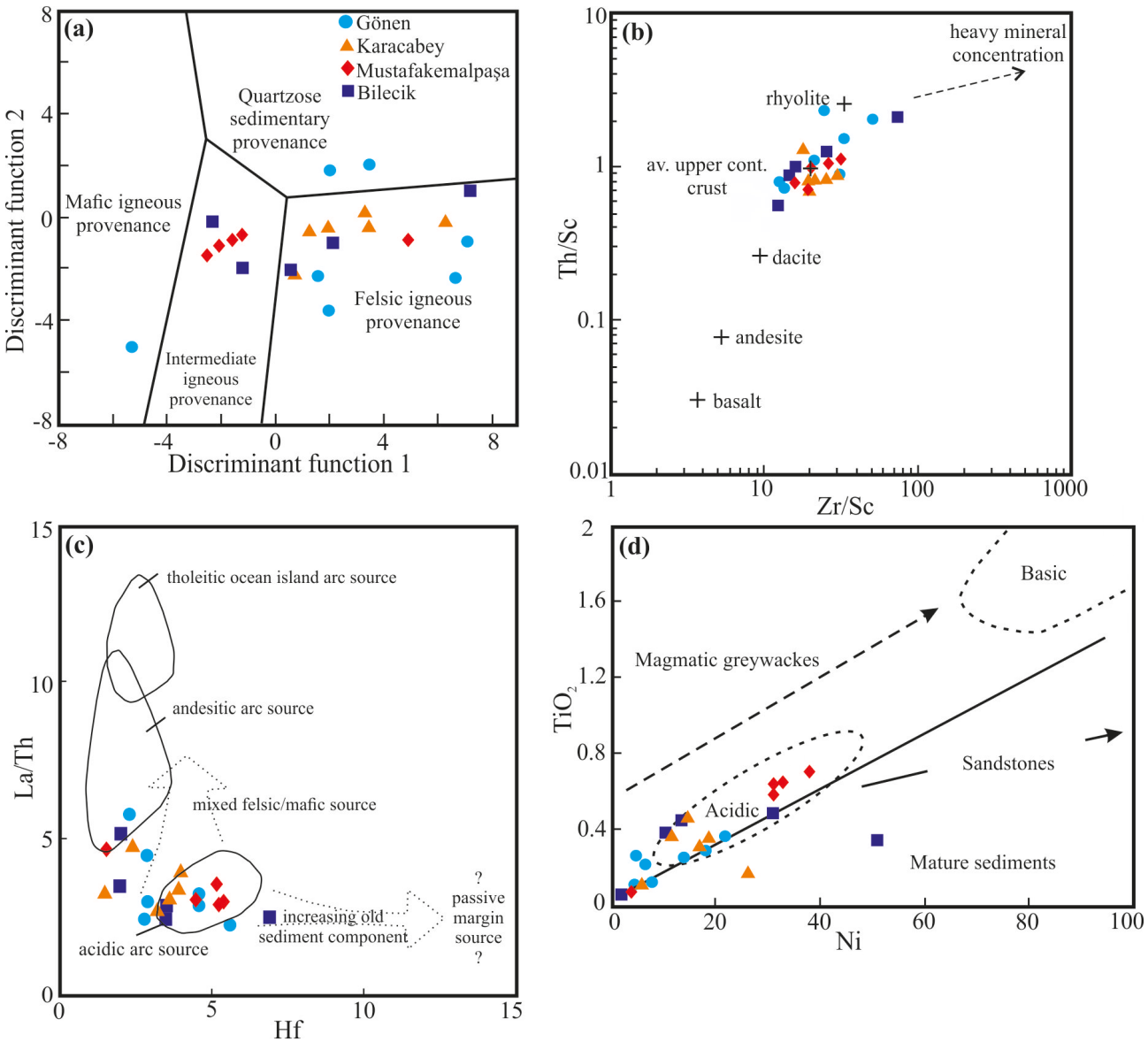

Figure 8. (a) Major element provenance discrimination diagram for sandstones (after Roser and Korsch, 1988). (b) Th/Sc vs. Zr/Sc plot for sandstone samples (after McLennan et al., 1993). (c) Source and composition discrimination diagram for sandstones using La/Th ratio and Hf concentrations (after Floyd and Leveridge, 1987). (d) TiO_2-Ni discrimination diagram showing the source and composition of sandstone samples (after Floyd et al., 1991).

Table 5. Selected elemental ratios of Jurassic sandstones from the Bayırköy Formation correlated with those of sediments derived from silicic and basic sources, UCC, and PAAS.

Location	Gönen[a]	Karacabey[a]	M. Kemal Paşa[a]	Bilecik[a]	Range of sediment from silicic sources[b]	Range of sediment from basic sources[b]	UCC[c]	PAAS[c]
Elemental ratio								
Eu/Eu*	0.61–0.77	0.69–0.90	0.59–0.76	0.50–0.86	0.40–0.94	0.71–0.95	0.63	0.60
La/Sc	3.0–4.63	2.17–4.60	2.52–5.50	2.0–11.0	2.50–16.30	0.43–0.86	2.21	2.50
Th/Sc	0.73–2.32	0.77–1.39	0.73–1.16	0.57–2.12	0.84–20.50	0.05–0.22	0.79	0.91
La/Co	2.77–18.50	2.70–7.03	1.98–3.67	0.75–11.00	1.80–13.80	0.14–0.38	1.76	1.65
Th/Co	0.73–8.11	0.85–1.79	0.65–0.84	0.21–2.12	0.67–19.40	0.04–1.40	0.63	0.63

[a] This study.
[b] Cullers (2000).
[c] Taylor and McLennan (1985).

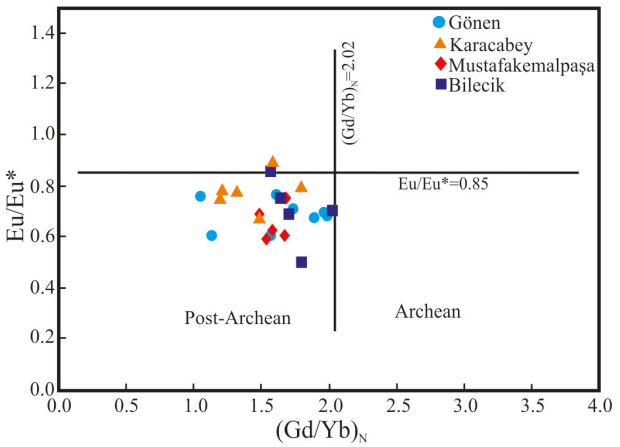

Figure 9. $(Gd/Yb)_N$ vs. Eu/Eu* plot of sandstone samples from the Bayırköy Formation (after McLennan and Taylor, 1991).

Felsic igneous rocks and metamorphic basement rocks are common within the western Sakarya Zone, which could be potential source rocks for sandstone samples from the Bayırköy Formation. All the plutonic rocks occurring on the basement of the Sakarya Zone have Carboniferous ages varying from 303 to 356 Ma (e.g., Okay et al., 2006; Topuz et al., 2010; Ustaömer et al., 2012b; Şengün and Koralay, 2017). This can be followed from the Biga Peninsula through the Central Sakarya Zone to the Eastern Sakarya Zone. The ages of plutonic rocks in the west of the Biga Peninsula vary between 334 Ma and 308 Ma (Carboniferous, Okay et al., 2006; Şengün and Koralay, 2017). The Central Sakarya basement is cut by the Söğüt granodiorite with Early Carboniferous age (319–327 Ma, Ustaömer et al., 2012a). Carboniferous magmatism (325–356 Ma) was documented from the eastern part of the Pontides (Ustaömer et al., 2012b). Permian granitoids are exposed commonly in the Central Sakarya Zone and dated as 275–298 Ma (Okay et al., 2006). In contrast to widespread Carboniferous magmatism, Devonian granitoids are rare and only occur in the Biga Peninsula. U-Pb zircon ages yield Early to Middle Devonian age for the Çamlık granodiorite (Aysal et al., 2012b). The age of another Devonian granitoid, the Karacabey Pluton, ranges from 393 Ma to 400 Ma (Sunal, 2012; Aysal et al., 2012a). These granitoids are often associated with medium to high-grade metamorphic basement rocks occurring in the Uludağ Massif, Kazdağ Massif, Kurtoğlu metamorphic complex, and Pulur Massif within the Sakarya Zone. The age of high-grade metamorphism in the western Sakarya Zone was determined as 310 Ma and 330 Ma based on U-Pb monazite and zircon ages (Okay et al., 1996; Topuz et al., 2010).

5.2. Tectonic setting

Chemical composition of clastic sedimentary rocks gives valuable information about the tectonic setting of depositional basins and is considerably controlled by the tectonic setting of their provenance. Therefore, major and trace element discrimination diagrams were used to discriminate tectonic settings of the sedimentary basin. Sandstone samples were plotted on the major element tectonic setting discrimination function diagram (Figure 10a). Most of the Jurassic sandstones, except those from the Gönen area, were deposited in a passive margin field (Figure 10a). Sandstones from the Gönen area plot on the active continental margin field. Sandstones falling within the passive continental margin could mainly have resulted from exposed areas and/or uplifted areas. La, Y, Th, Sc, and Zr are immobile trace elements that are widely used to reveal the tectonic setting of sedimentary rocks. The Sc/Cr vs. La/Y diagram shows that the sandstones fall into the passive and active continental field (Figure 10b). This is in accordance with the diagram proposed by Bhatia (1983) in Figure 10a. The Th-Co-Zr/10 triangular diagram plot

is commonly used to distinguish sandstones derived from distinct tectonic settings and source areas (Figure 10c). The plot of Th-Co-Zr/10 shows that some sandstones from the Gönen area fell in the field of the passive continental margin, whereas the rest were deposited in continental island arc settings. New multidimensional diagrams (Verma and Armstrong-Altrin, 2013) were used for the tectonic discrimination of siliciclastic sedimentary rocks based on integrated major and trace elements. Three main tectonic settings were produced on these diagrams, which comprise continental and/or island arc, continental collision, and rift. A new major element discrimination diagram (Figure 10d) was used to decipher the tectonic setting of the Jurassic sandstones from the Bayırköy Formation. The Jurassic sandstones mostly fell in the rift field based on the tectonic discriminant high-silica [$(SiO_2)_{adj} \geq 63\%$ to $\leq 95\%$] diagram. However, a few samples fell in the collision field.

All tectonic discrimination diagrams indicate that the Jurassic sandstones from the Bayırköy Formation fall in the fields of 2 different tectonic settings rather than plotting in a certain tectonic setting field. However, the field of marginal basin opening behind overlying crust during subduction of the oceanic crust is not included in these diagrams. Subduction-related marginal basins are structurally similar to passive marginal basins but are separated by magmatism occurring on one of the margins. Therefore, marginal basins are a kind of transitional

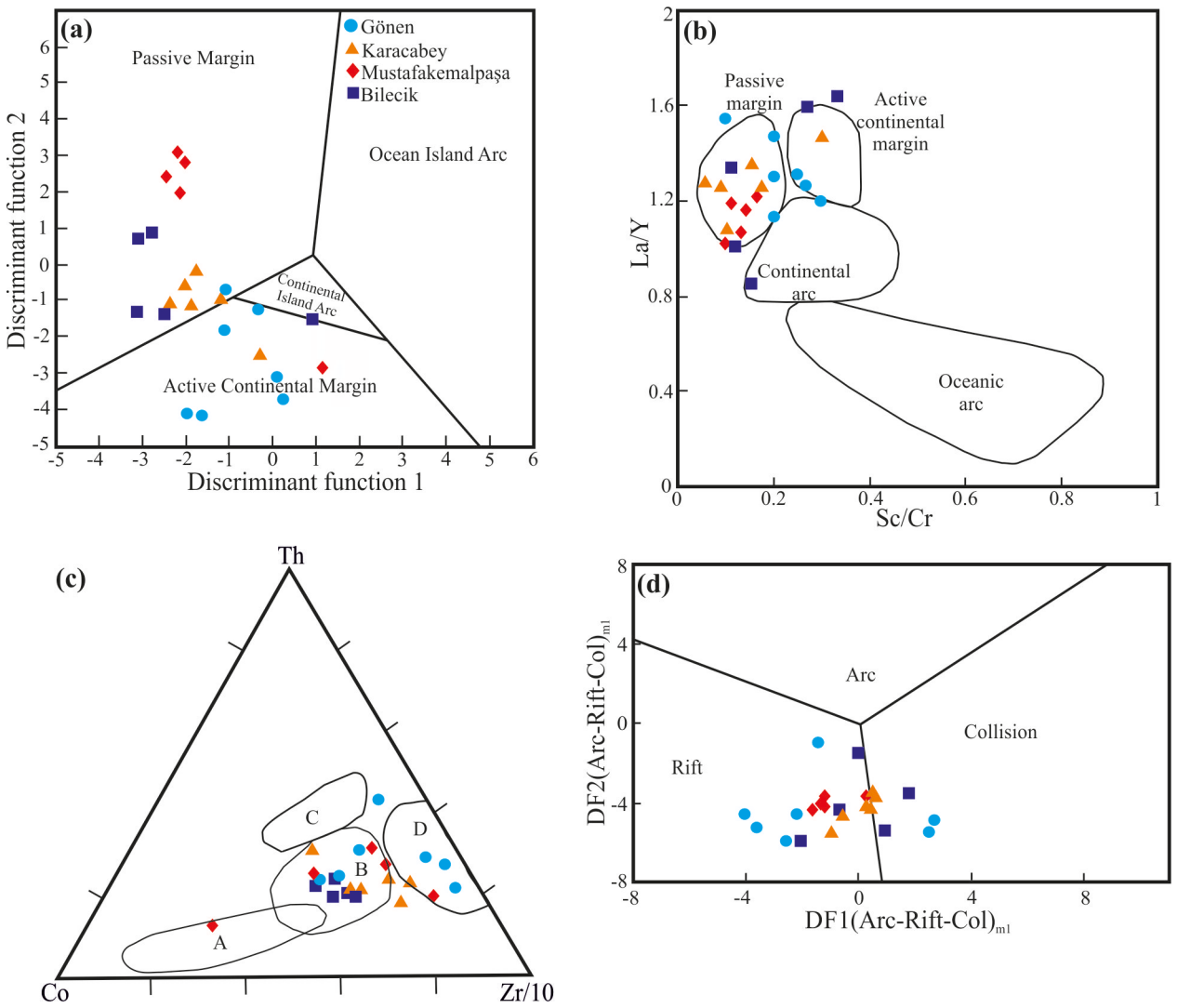

Figure 10. (a) Discriminant function diagram for Jurassic sandstones (after Bhatia, 1983). (b) The plot of Sc/Cr vs. La/Y (after Bhatia and Crook, 1986). (c) Th-Co-Zr/10 triangular diagram (after Bhatia and Crook, 1986; A: Oceanic island arc, B: Continental island arc, C: Active continental margin, D: Passive margin). (d) New discriminant function multidimensional diagram for high-silica clastic sediments (after Verma and Armstrong-Altrin, 2013).

basin between continental marginal basins and passive marginal basins from this aspect, which naturally affects the sedimentation. The Jurassic sandstones exposed in the western part of the Sakarya Zone, except those in the Gönen area, have the characteristic features of passive continental margin basins. Some samples have high felsic constituents, like K_2O, Th, Zr, and La, indicating a passive continental margin. The Early Jurassic basins formed on passive continental margins located south of a subduction-related magmatic arc. Sediments derived from the rifting basement rocks (metamorphic and granitic rocks) were transferred into the back-arc basin and define the tectonic setting as having the characteristics of a passive continental margin.

5.3. Weathering in source area and climate

Chemical weathering intensity of source rocks influences the geochemistry of major elements and the mineralogical composition, and is monitored by physical sorting and climatic conditions (McLennan, 1993). The chemical index of weathering (CIW) and chemical index of alteration (CIA) are the most commonly used chemical indices for evaluating chemical weathering degree in source areas. CIW and CIA values are given in Table 3. The high CaO-content samples may cause misleading results when CIA and CIW are used to infer the degree of weathering (Cullers, 2000). The CaO content of the Jurassic sandstone samples ranges between 0.21 and 16.80 wt.%. Thus, the high CaO concentration was corrected following the method of McLennan (1993) to separate CaO content in silicate composition (CaO*) and nonsilicate composition. The degree of chemical weathering is classified as low (CIA values between 50 and 60), moderate (CIA values between 60 and 80), and intense (CIA values above 80) (Nesbitt and Young, 1982). However, CIA values for the Jurassic sandstones vary from 58 to 77 (average: 68) and indicate that chemical weathering has low to moderate intensity in the source regions (Figure 11a). However, CIW values vary between 79 and 96 (average: 86). These high values could suggest that unstable plagioclase disintegrated during diagenesis or transportation rather than by intense chemical weathering in the source area (Tawfik et al., 2017).

The compositional changes during chemical weathering processes and source rock composition can be revealed by the Al_2O_3-(CaO^*+Na_2O)-K_2O (A-CN-K) triangular diagram. On the A-CN-K ternary diagram (Figure 11a), sandstones mostly plot in the intermediate field, which shows removal of Ca and Na because of plagioclase destruction (Buggle et al., 2008; Ahmad and Chandra, 2013). Moreover, weathering trends can state the average chemical composition of the source rocks. These trends result from distinct element mobilities during surface weathering. Fe and Mg elements together with Ca and Na elements are the least resistant and most mobile elements in silicates. However, K is less mobile but Al is rather immobile (Nesbitt and Young, 1984). The ternary diagram of A-CN-K shows that the Jurassic sandstones originated from a dioritic to granitic source (Figure 11a).

Climate influences sandstone composition through its destructive effect on source rocks. The SiO_2 vs. total Al_2O_3+K_2O+Na_2O diagram indicates different climate heritages for sandstone samples (Figure 11b). The major-

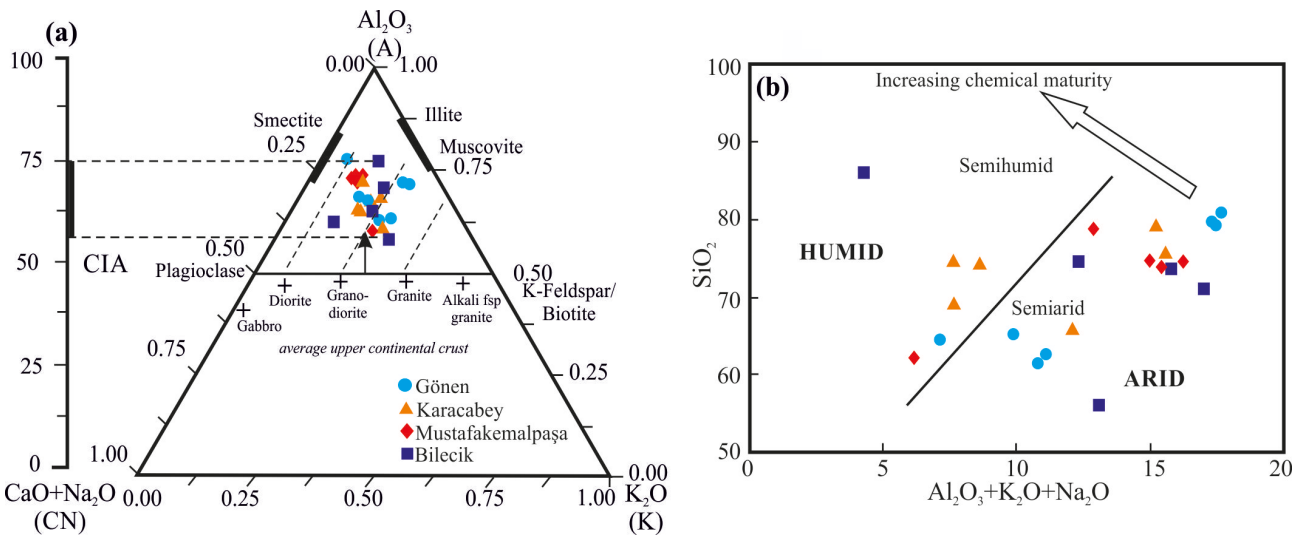

Figure 11. (a) A-CN-K ternary diagram for Jurassic sandstones of the Bayırköy Formation (after Nesbitt and Young, 1984). The average chemical composition of the source area is shown by weathering trends for magmatic source rocks. (b) Chemical maturity of the Jurassic sandstones (after Suttner and Dutta, 1986).

element concentrations demonstrate that the Jurassic sandstones formed under mostly semihumid and semiarid climatic conditions.

6. Conclusions

The Jurassic clastic rocks from the Bayırköy Formation occur widely in the western part of the Sakarya Zone. Integrated geochemical (major, trace, REE elements) and petrographic studies of the Jurassic sandstones provided significant information about the provenance, source terrains, tectonic setting, intensity of weathering, and climatic conditions in the Sakarya Zone. The Bayırköy Formation is dominantly composed of sandstones with shale, claystone interbeds, and rarely conglomerate. The Jurassic sandstones are mainly classified as litharenite, subarkose, and arkose according to petrographic analyses and major element geochemistry. Various tectonic discrimination diagrams for major and trace elements suggest that the Jurassic sandstones, except those within the Gönen area, could have been deposited in a passive continental margin. It can be noted that sandstones may have been deposited in a marginal basin that began to open in Early Jurassic time. Felsic igneous rocks and metamorphic basement rocks commonly occur in the western Sakarya Zone, which could be the potential source rocks for Jurassic sandstones from the Bayırköy Formation. These felsic rocks have ages ranging from Devonian to Permian in the Sakarya Zone. The Jurassic sandstones chiefly originated from felsic to intermediate source rocks (i.e. granite to diorite). The enrichment of Zr and the negative Eu anomaly suggest that mafic input was not transferred into the depositional area. CIW and CIA values reveal that the source area experienced low to moderate chemical weathering under semihumid to semiarid climate conditions.

Acknowledgments

The Scientific Research Coordination Unit of Çanakkale Onsekiz Mart University supported this study with project number FHD-2016-1086. We thank the editor, Timur Ustaömer, for his constructive comments. Constructive reviews by Aral Okay, Sema Tetiker, and an anonymous reviewer helped to clarify the picture and considerably improved the manuscript.

References

Ahmad I, Chandra R (2013). Geochemistry of loess-paleosol sediments of Kashmir Valley, India: provenance and weathering. J Asian Earth Sci 66: 73-89.

Akdoğan R, Okay AI, Dunkl I (2018). Triassic-Jurassic arc magmatism in the Pontides as revealed by the U-Pb detrital zircon ages in the Jurassic sandstones of northeastern Turkey. Turkish J Earth Sci 27: 89-109.

Akdoğan R, Okay AI, Sunal G, Tari G, Meinhold G, Kylander-Clark ARC (2017). Provenance of a large Lower Cretaceous turbidite submarine fan complex on the active Laurasian margin. J Asian Earth Sci 134: 309-329.

Akyürek B, Duru, M, Sütçü YF, Papak İ, Şaroğlu F, Pehlivan N, Gönenç O, Granit S, Yaşar T (1996). Ankara İlinin Çevre Jeolojisi ve Doğal Kaynaklar Projesi. MTA Report No: 9961. Ankara, Turkey: MTA (in Turkish).

Altıner D, Koçyiğit A, Farinacci A, Nicosia U, Conti MA (1991). Jurassic, Lower Cretaceous stratigraphy and paleogeographic evolution of the southern part of north-western Anatolia. Geol Romana 28: 13-80.

Altınlı İE (1973). The Geology of middle Sakarya. In: Congress Proceedings of the Earth Sciences 50th Anniversary of the Turkish Republic, Mineral Research Exploration Institute (MTA), Ankara, pp. 159-191 (in Turkish).

Asiedu DK, Suzui S, Shibata T. (2000). Provenance of sandstones from the Lower Cretaceous Sasayama Group, inner zone of southwest Japan. Sediment Geol 131: 9-24.

Aysal N, Öngen S, Peytcheva I, Keskin M (2012a). Origin and evolution of the Havran Unit, Western Sakarya basement (NW Turkey): new LA-ICP-MS U-Pb dating of the metasedimentary-metagranitic rocks and possible affiliation to Avalonian microcontinent. Geodin Acta 25: 226-247.

Aysal N, Ustaömer T, Öngen S, Keskin M, Köksal S, Peytcheva I, Fanning M (2012b). Origin of the Early-Middle Devonian Magmatism in the Sakarya Zone, NW Turkey: geochronology, geochemistry and isotope systematics. J Asian Earth Sci 45: 201-222.

Basu A, Bickford ME, Deasy R (2016). Inferring tectonic provenance of siliciclastic rocks from their chemical compositions: a dissent. Sediment Geol 336: 26-35.

Bhatia MR (1983). Plate tectonics and geochemical composition of sandstones. J Geol 91: 611-627.

Bhatia MR, Crook KAW (1986). Trace element characteristics of greywackes and tectonic setting discrimination of sedimentary basins. Contrib Mineral Petr 92: 181-193.

Borges JG, Gus Y, Moon S, Noh H (2008). Provenance and weathering control on river bed sediments of the eastern Tibetan Plateau and the Russian Far East. Chem Geol 254: 52-72.

Buggle B, Glaser B, Zoller L, Hambach U, Markovic S, Glaser I, Gerasimenko N (2008). Geochemical characterization and origin of Southeastern and Eastern European loess (Serbia, Romania, Ukraine). Quaternary Sci Rev 27: 1058-1075.

Cox R, Lowe DR, Cullers RL (1995). The influence of sediment recycling and basement composition on evolution of mudrock chemistry in the southwestern United States. Geochim Cosmochim Ac 59: 2919-2940.

Critelli S, Arribas J, Le Pera E, Tortosa A, Marsaglia KM, Latter KK (2003). The recycled orogenic sand provenance from an uplifted thrust belt, Betic Cordillera, Southern Spain. J Sediment Res 73: 72-81.

Cullers RL (2000). The geochemistry of shales, siltstones and sandstones of Pennsylvanian–Permian age, Colorado, U.S.A.: implications for provenance and metamorphic studies. Lithos 51: 181-203.

Dickinson WR (1970). Interpreting detrital modes of graywackes and arkose. J Sediment Geol 40: 695-707.

Dickinson WR, Suczek CA (1979). Plate tectonics and sandstone compositions. Am Assoc Petr Geol B 63: 2164-2182.

Dokuz A (2011). A slab detachment and delamination model for the generation of Carboniferous high potassium I-type magmatism in the Eastern Pontides, NE Turkey: Köse composite pluton. Gondwana Res 19: 926-944.

Duru M, Gedik İ, Aksay A (2002). 1/100000-scale Geological Map Series of Turkey, Adapazarı-H24 Sheet, No: 37. Ankara, Turkey: General Directorate of Mineral Research and Exploration (in Turkish).

Floyd PA, Leveridge BE (1987). Tectonic environment of the Devonian Gramscatho basin, south Cornwall: framework mode and geochemical evidence from turbiditic sandstones. Geol Soc Spec Publ 144: 531-542.

Floyd PA, Shail R, Leveridge BE, Franke W (1991). Geochemistry and provenance of Rhenohercynian synorogenic sandstones: implications for tectonic environment discrimination. Geol Soc Spec Publ 57: 173-188.

Garzanti E, Padoan M, Andò S, Resentini A, Vezzoli G, Lustrino M (2013). Weathering and relative durability of detrital minerals in equatorial climate: and petrology and geochemistry in the East African Rift. J Geol 121: 547-580.

Ghosh S, Sarkar S (2010). Geochemistry of Permo-Triassic mudstone of the Satpura Gondwana Basin, Central India: clues for provenance. Chem Geol 277: 78-100.

Hara H, Kunii M, Hisada K, Ueno K, Kamata Y, Srichan, W, Charusiri P, Charoentitrat T, Watarai M, Adachi Y et al. (2012). Petrography and geochemistry of clastic rocks within the Inthanon zone, northern Thailand: implications for Paleo-Tethys subduction and convergence. J Asian Earth Sci 61: 2-15.

Harnois L (1988). The CIW index: a new chemical index of weathering. Sediment Geol 55: 319-322.

Ingersoll RV, Bullard TF, Ford RL, Grimm JP, Pickle JD, Sares SW (1984). The effect of grain size on detrital modes: a test of the Gazzi-Dickinson point-counting method. J Sediment Petrol 54: 103-116.

Kandemir Ö, Pehlivan Ş, Kanar F, Tok T (2013). 1/100000-Scaled Geological Map Series of Turkey, Bandırma-H21 Sheet, No: 191. Ankara, Turkey: General Directorate of Mineral Research and Exploration (in Turkish).

Kaygusuz A, Arslan M, Sipahi F, Temizel İ (2016). U–Pb zircon chronology and petrogenesis of Carboniferous plutons in the northern part of the Eastern Pontides, NE Turkey: constraints for Paleozoic magmatism and geodynamic evolution. Gondwana Res 39: 327-346.

Kretz R (1983). Symbols of rock-forming minerals. Am Mineral 68: 277-279.

Lewis DM, McConchie D (1994). Practical Sedimentology. New York, NY, USA: Chapman and Hall.

Löwen K, Meinhold G, Güngör T (2018). Provenance and tectonic setting of Carboniferous–Triassic sandstones from the Karaburun Peninsula, western Turkey: a multi-method approach with implications for the Palaeotethys evolution. Sediment Geol 375: 232-255.

McBride EF (1963). A classification of common sandstones. J Sediment Petrol 33: 664-669.

McCann T (1991). Petrological and geochemical determination of provenance in the southern Welsh Basin. Geol Soc Spec Publ 57: 215-230.

McLennan SM (1989). Rare earth elements in sedimentary rocks; influence of provenance and sedimentary processes. Rev Mineral 21: 169-200.

McLennan SM (1993). Weathering and global denudation. J Geol 101: 295-303.

McLennan SM, Hemming DK, Hanson GN (1993). Geochemical approaches to sedimentation, provenance and tectonics. Geol S Am S 284: 21-40.

McLennan SM, Taylor SR (1991). Sedimentary rocks and crustal evolution: tectonic setting and secular trends. J Geol 99: 1-21.

Meinhold G, Kostopoulos D, Frei D, Himmerkus F, Reischmann T (2010). U-Pb LA-SF ICP-MS zircon geochronology of the Serbo-Macedonian Massif, Greece: Palaeotectonic constraints for Gondwana-derived terranes in the Eastern Mediterranean. Int J Earth Sci 99: 813-832.

Morton AC, Hallsworth C (1994). Identifying provenance-specific features of detrital heavy mineral assemblages in sandstones. Sediment Geol 90: 241-256.

Nesbitt HW, Young GM (1982). Early Proterozoic climates and plate motion inferred from major element chemistry of lutites. Nature 299: 715-717.

Nesbitt HW, Young GM (1984). Prediction of some weathering trends of plutonic and volcanic rocks based on thermodynamic and kinetic considerations. Geochim Cosmochim Ac 48: 1523–1534.

Okay Aİ, Göncüoğlu MC (2004). The Karakaya Complex: a review of data and concepts. Turkish J Earth Sci 13: 77-95.

Okay AI, Satır M, Maluski H, Siyako M, Monie P, Metzger R, Akyüz S (1996). Paleo and Neotethyan events in northwest Turkey. In: Yin A, Harrison M, editors. Tectonics of Asia. Cambridge, UK: Cambridge University Press, pp. 420-441.

Okay AI, Satir M, Siebel W (2006). Pre-Alpide and Mesozoic orogenic events in the Eastern Mediterranean region. Geol Soc Spec Publ 32: 389-405.

Okay AI, Tüysüz O (1999). Tethyan sutures of northern Turkey. Geol Soc Spec Publ 156: 475-515.

Periasamy V, Venkateshvarlu M (2017). Petrography and geochemistry of Jurassic sandstones from the Jhuran Formation of Jara dome, Kachchh basin, India: implications for provenance and tectonic setting. J Earth Syst Sci 126: 44.

Pettijohn FJ, Potter PE, Siever R (1972). Sand and Sandstone. New York, NY, USA: Springer Verlag.

Roser BP, Korsch RJ (1986). Determination of tectonic setting of sandstone–mudstone suites using SiO_2 content and K_2O/Na_2O ratio. J Geol 94: 635-650.

Roser BP, Korsch RJ (1988). Provenance signatures of sandstone–mudstone suites determined using discriminant function analysis of major-element data. Chem Geol 67: 119-139.

Saydam Eker C (2012). Petrography and geochemistry of Eocene sandstones from Eastern Pontides (NE Turkey): implications for source area weathering, provenance and tectonic setting. Geochem Int+ 50: 683-701.

Saydam Eker C, Korkmaz S (2011). Mineralogy and whole-rock geochemistry of late Cretaceous sandstones from the eastern Pontides (NE Turkey). Neues Jb Miner Abh 188: 235-256.

Stunner LJ, Basu A (1985). The effect of grain size on detrital modes: a test of the Gazzi-Dickinson point-counting method discussion. J Sediment Petrol 55: 616-627.

Sunal G (2012). Devonian magmatism in the western Sakarya Zone, Karacabey Region, NW Turkey. Geodin Acta 25: 183-201.

Suttner LJ, Dutta PK (1986). Alluvial sandstone composition and paleoclimate, I. Framework mineralogy. J Sediment Petrol 56: 329-345.

Şengün F (2019). U-Pb Detrital Zircon Geochronology of Sandstones from the North of Gönen County (Balıkesir). Project No: FBA-2019-2868. Çanakkale, Turkey: Çanakkale Onsekiz Mart University Scientific Research Coordination Unit (in Turkish).

Şengün F, Koralay OE (2017). Early Variscan magmatism along the southern margin of Laurasia: geochemical and geochronological evidence from the Biga Peninsula, NW Turkey. Int J Earth Sci 106: 811-826.

Tawfik HA, Ghandour IM, Maejimas W, Armstrong-Altrin JS, Abdel-Hameed AT (2017). Petrography and geochemistry of the siliciclastic Araba Formation (Cambrian), east Sinai, Egypt: implications for provenance, tectonic setting and source weathering. Geol Mag 154: 1-23.

Taylor SR, McLennan SM (1985). The Continental Crust: Its Composition and Evolution. Oxford, UK: Blackwell.

Tetiker S (2010). Geochemistry properties and origin of metasandstones in the Karakaya Complex units (NW Anatolia and Tokat area). Cumhuriyet University Bulletin of the Faculty of Engineering Series A 26: 1-22 (in Turkish with abstract in English).

Topuz G, Altherr R, Kalt A, Satır M, Werner O, Schwarz WH (2004). Aluminous granulites from the Pulur complex, NE Turkey: a case of partial melting, efficient melt extraction and crystallization. Lithos 72: 183-207.

Topuz G, Altherr R, Schwarz WH, Dokuz A, Meyer H (2007). Variscan amphibolite-facies rocks from the Kurtoğlu Metamorphic Complex (Gümüşhane Area, Eastern Pontides, Turkey). Int J Earth Sci 96: 861-873.

Topuz G, Altherr R, Siebel W, Schwarz WH, Zack T, Hasözbek A, Barth M, Satır M, Şen C (2010). Carboniferous high-potassium I-type granitoid magmatism in the Eastern Pontides: the Gümüşhane pluton (NE Turkey). Lithos 116: 92-110.

Tucker ME (1991). Sedimentary Petrology. Oxford, UK: Blackwell Scientific Publications.

Ustaömer PA, Ustaömer T, Gerdes A, Robertson AHF, Collins AS (2012a). Evidence of Precambrian sedimentation/magmatism and Cambrian metamorphism in the Bitlis Massif, SE Turkey utilizing whole-rock geochemistry and U–Pb LA-ICP-MS zircon dating. Gondwana Res 21: 1001-1018.

Ustaömer PA, Ustaömer T, Robertson AHF (2012b). Ion probe U-Pb dating of the Central Sakarya Basement: a peri-Gondwana terrane intruded by late Lower Carboniferous subduction/collision-related granitic rocks. Turkish J Earth Sci 21: 905-932.

Ustaömer T, Robertson AHF (2010). Late Palaeozoic–Early Cenozoic tectonic development of the Eastern Pontides (Artvin area), Turkey: stages of closure of Tethys along the southern margin of Eurasia. Geol Soc Spec Publ 340: 281-327.

Ustaömer T, Ustaömer PA, Robertson AHF, Gerdes A (2016). Implications of U-Pb and Lu–Hf isotopic analysis of detrital zircons for the depositional age, provenance and tectonic setting of the Permian-Triassic Palaeotethyan Karakaya Complex, NW Turkey. Int J Earth Sci 105: 7-38.

Verma SP, Armstrong-Altrin JS (2013). New multidimensional diagrams for tectonic discrimination of siliciclastic sediments and their application to Precambrian basins. Chem Geol 355: 117-133.

von Eynatten H, Tolosana-Delgado R, Karius V (2012). Sediment generation in modern glacial settings: Grain-size and source-rock control on sediment composition. Sediment Geol 280: 80-92.

Yiğitbaş E, Şengün F, Tunç İO (2009). Distribution and Correlation of Mesozoic Rock Assemblages of NW Anatolia. TÜBİTAK Report, Project No; ÇAYDAG 108Y232. Ankara, Turkey: TUBTAK (in Turkish).

Young SM, Pitawala A, Ishiga H (2013). Geochemical characteristics of stream sediments, sediment fractions, soils, and basement rocks from the Mahaweli River and its catchment, Sri Lanka. Chem Erde-Geochem 73: 357-371.

Zaid SM, Elbadry O, Ramadan F, Mohamed M (2015). Petrography and geochemistry of Pharaonic sandstone monuments in Tall San Al Hagr, Al Sharqiya Governorate, Egypt: implications for provenance and tectonic setting. Turkish J Earth Sci 24: 344-64.